ChemPlusChem

Research Article
doi.org/10.1002/cplu.202300411

Chemistry Europe
European Chemical Societies Publishing

www.chempluschem.org

Special Collection

Enhancing Hydrogen Production from the Photoreforming of Lignin

Meshal Aljohani,[a, b] Helen Daly,*[a] Lan Lan,[a] Aristarchos Mavridis,[a] Matthew Lindley,[c] Sarah J. Haigh,[c] Carmine D'Agostino,[a] Xiaolei Fan,*[a] and Christopher Hardacre*[a]

Photoreforming of lignocellulose biomass is widely recognised as a challenging but key technology for producing value-added chemicals and renewable hydrogen (H_2). In this study, H_2 production from photoreforming of organosolv lignin in a neutral aqueous solution was studied over a 0.1 wt% Pt/TiO_2 (P25) catalyst with ultraviolet A (UVA) light. The H_2 production from the system employing the lignin (~4.8 $\mu mol\, g_{cat}^{-1}\, h^{-1}$) was comparable to that using hydroxylated/methoxylated aromatic model compounds (i.e., guaiacol and phenol, 4.8–6.6 $\mu mol\, g_{cat}^{-1}\, h^{-1}$), being significantly lower than that from photoreforming of cellulose (~62.8 $\mu mol\, g_{cat}^{-1}\, h^{-1}$). Photoreforming of phenol and reaction intermediates catechol, hydroquinone and benzoquinone were studied to probe the mechanism of phenol oxidation under anaerobic photoreforming conditions with strong adsorption and electron transfer reactions lowering H_2 production from the intermediates relative to that from phenol. The issues associated with catalyst poisoning and low photoreforming activity of lignins demonstrated in this paper have been mitigated by implementing a process by which the catalyst was cycled through anaerobic and aerobic conditions. This strategy enabled the periodic regeneration of the photocatalyst resulting in a threefold enhancement in H_2 production from the photoreforming of lignin.

Introduction

Global energy requirements are projected to increase 65% by 2030 compared to the energy production level of 2010. Currently, fossil fuels are the primary sources for both energy production (at >80% of global energy) and the production of chemicals, which brings significant environmental problems from carbon emission and the associated global warming.[1] Hydrogen (H_2) with a calorific value of 141.8 $MJ\, kg^{-1}$ (which is approximately three times that of hydrocarbon fuels, e.g., 50–55 $MJ\, kg^{-1}$ for methane) is a promising clean energy and is considered as a major candidate in the move away from fossil fuel-based energy.[2] However, more than 90% of hydrogen production comes from fossil fuels, mainly from steam methane reforming, which requires harsh conditions of typically 700–900 °C and 20–35 atm. Moreover, decarbonisation of H_2 production (via steam reforming processes) requires additional unit operation for CO_2 capture with utilisation and/or storage (CCUS).[2–3] Therefore, sustainable alternatives for renewable H_2 production are urgently needed to answer the ever-increasing energy demand and mitigate the environmental impact of established, fossil-fuel based H_2 production technologies.

Solar-driven photocatalytic reforming of biomass under ambient conditions presents a promising technology for the production of renewable H_2 and platform chemicals/fuels[4] due to the use of (i) biomass resources (widely abundant in nature, sustainable and theoretically carbon neutral) and (ii) solar energy (i.e., the sun as the largest energy resource to drive the catalysis).[4] Hence, photoreforming which can utilise biomass, biomass wastes streams or renewable feedstocks can potentially play an important role in future sustainable H_2 production.[5]

Lignocellulose is the most abundant source of biomass on earth, which is composed of polymeric carbohydrates such as cellulose (40–50%), hemicellulose (20–30%) and lignin (10–25%).[6] For example, it is estimated that the annual lignin production could reach 36×10^8 tons[7] and be a promising source of fuels and valuable products as an alternative to fossil fuels[8] if suitable conversion technologies are developed. Although photoreforming of cellulose and hemicellulose has been demonstrated to provide higher H_2 production than from lignins, its significant proportion in the composition of biomass means that it has the potential to increase the overall H_2 yield if improvements in its photoreforming can be achieved.[5]

[a] M. Aljohani, Dr. H. Daly, Dr. L. Lan, A. Mavridis, Dr. C. D'Agostino, Dr. X. Fan, Prof. C. Hardacre
Department of Chemical Engineering
The University of Manchester
Oxford Road, Manchester M13 9PL (UK)
E-mail: helen.daly@manchester.ac.uk
xiaolei.fan@manchester.ac.uk
c.hardacre@manchester.ac.uk

[b] M. Aljohani
The Center of Excellence for Advanced Materials and Manufacturing
King Abdulaziz City for Science and Technology
Riyadh 11442 (Saudi Arabia)

[c] Dr. M. Lindley, Prof. S. J. Haigh
Department of Materials
The University of Manchester
Oxford Road, Manchester M13 9PL (UK)

Supporting information for this article is available on the WWW under https://doi.org/10.1002/cplu.202300411

Special Collection Part of a Special Collection on Green Chemistry

Photoreforming of biomass-derived sugars and polyols such as glucose,[9] glycerol[10] and cellulose[11] has been widely studied; however, lignin as a substrate in photoreforming has received much less attention since the first report in 1980 by Kawai and Sakata.[12] Therein, using a Pt/TiO_2 catalyst, the production of H_2 from photoreforming of lignin was 77 μmol for reaction in 5 M NaOH aqueous solution compared to 12 μmol in water, both after 10 hours of UV irradiation, which was significantly lower than the H_2 production from the system using cellulose as the substrate where 200 μmol H_2 was produced in 5 M NaOH solution.

Photoreforming of simple, water-soluble organic molecules such as alcohols and sugars provides the highest H_2 production. In contrast, lignin has a complex structure, is insoluble in water, and is hydrophobic in nature. In addition, the chromophoric functionalities in lignin, responsible for its brown colour, can absorb light of wavelengths >300 nm, which could reduce the available light for absorption by the photocatalyst. The H_2 production from the photoreforming of lignin is presented in Table 1 where, to date, lignin photoreforming for H_2 production has predominantly been implemented in an alkaline[12–13] or acidic medium[13b,14] to improve the solubility/decomposition of lignin.

High H_2 production from lignin has been achieved but only under alkaline conditions, whilst significantly lower H_2 was produced in acid or neutral reaction media. Wakerley et al.[13a] showed that lignin decomposed in 10 M KOH solution under UV irradiation regardless of the presence of a catalyst, whilst H_2 was only formed in the presence of a catalyst. The decomposition of lignin (irradiation over 5 days), therein, was probed by UV-visible diffuse reflectance (UV-Vis) spectroscopy, showing the oxidation of phenols within the lignin to quinones. Lignin decomposition was also studied by Zhao et al. in photoreforming of lignin in aqueous lactic acid solution[13c] wherein, UV-Vis spectroscopy showed that the lignin chromophoric functionalities were depleted after reaction. In addition, heteronuclear single quantum correlation nuclear magnetic resonance (HSQC NMR) signals from linkages such as β-O-4, β-β, and β-5 decreased after reaction, indicating depolymerisation of lignin or release of aromatic groups from lignin's structure.

While higher H_2 production from lignin under alkaline conditions has been linked to increased decomposition of lignin, the nature of the substrate being reformed to H_2 (undergoing oxidative reactions with OH radicals/photogenerated holes) on the catalyst surface has not been discussed in detail. Alkali catalysed decomposition of lignin can result in higher molecular weight polymers from the condensation (repolymerisation) of unstable lignin fragments in solution. The condensed lignin can be of a more recalcitrant nature as the β-O-4 linkages are removed in the degradation of lignin with the condensed lignin having a greater portion of lower activity C–C linkages.[15] The system can be further complicated by polymerisation of monomer phenolic compounds.[16] The attribution of improved H_2 production under alkaline conditions with increased lignin solubility does not address the complexity of the system, and lignin decomposition products could be important in the photoreforming mechanism particularly if they interact with the catalyst surface in preference to the oligomer/polymer chains.

Herein, catalytic photoreforming was performed over a 0.1% Pt/TiO_2 P25 catalyst in water under neutral, ambient conditions. The H_2 production from the photocatalytic reforming of organosolv lignin was compared with cellulose (as a component of lignocellulose), as well as guaiacol and phenol (as lignin monomer model compounds), to benchmark the H_2 production of the system. Phenol oxidation intermediates were also investigated as substrates for photoreforming to understand the oxidation pathway and the overall efficiency of photocatalytic H_2 production in aromatic systems.

Table 1. State-of-the-art photocatalytic lignin reforming systems and the performance.

Photocatalyst	Light source	P/I (W)/(mW cm^{-2})	Concentration ($g\,L^{-1}$)		H_2 production ($\mu mol\,h^{-1}\,g_{cat}^{-1}$)	Ref.
			Catalyst	Substrate		
Pt/TiO_2	Xe	500/–	10	3.3	4	[12]
Pt/TiO_2	Xe	500/–	10	3.3/5 M NaOH	256.6	[12]
CdS/CdO_x QDs	Solar Simulator	–/100	0.5[a]	0.25/10 M KOH	260[b]	[13a]
NiP/ $^{NCN}CN_x$	Solar Simulator	–/100	1.6	0.16/4.3 M potassium phosphate	40.8	[13b]
Pt/$^{NCN}CN_x$	Solar Simulator	–/100	1.6	0.16/10 M KOH	14.5	[13b]
TiO_2/NiO	Xe	300/–	0.5	0.4/1 M NaOH	450[c]	[13c]
Pt/g-C_3N_4	Xe	300/100	5	5/pH = 10	20.75	[13d]
NiS/CdS	Xe	300/–	1	0.1/lactic acid	426.5[b,d]	[14]
Cu–In/ZnS	Solar Simulator	–/100	10	20/10 M NaOH	1.9	[13e]
Pt/C_3N_4	Blue LED	40/–	2	20/10 M NaOH	310	[13f]

[a] The catalysts concentration = 0.5 μM [b] Apparent Quantum Yield (AQY %) for[13a] = 1.2 and for[14] = 44.9; [c] Other products were also identified including CH_4 and fatty acids (palmatic and stearic acids major species); [d] H_2 production rate of 1512.4 $\mu mol\,h^{-1}\,g_{cat}^{-1}$ for lignin + lactic acid aqueous solution and 1085.9 $\mu mol\,h^{-1}\,g_{cat}^{-1}$ for the lactic acid aqueous solution without lignin. 426.5 $\mu mol\,h^{-1}\,g_{cat}^{-1}$ H_2 production attributed to the addition of lignin to the system.

Results and Discussion

Physicochemical properties of the catalyst

PXRD patterns of the P25 TiO_2 support and the Pt/TiO_2 catalyst are shown in Figure S1 in the Supplementary Information (SI). XRD patterns of the TiO_2 support consisted of mixed phases of anatase and rutile with the prominent diffraction peak for the anatase phase at $2\theta = 25.3°$ (101 reflections) and for the rutile phase at $2\theta = 27.4°$ (110 reflections). The average percentage ratio of anatase to rutile in the P25 TiO_2 support was determined to be 81:19 (Table S1), being consistent with previously reported values.[17] The XRD pattern of Pt/TiO_2 was similar to that of the TiO_2 support, and relevant Pt diffraction peaks were not identified due to the low Pt loading (of about 0.1 wt%, by ICP-OES) and/or the presence of ultrasmall (< 4 nm) and highly dispersed Pt nanoparticles.[9b,18] STEM analysis of the particles size distribution showed Pt particles with an equivalent circular diameter of 1.0 ± 0.4 nm (Figure S2). The average anatase and rutile crystallite size remained unchanged after Pt loading on the TiO_2 support, as shown in Table S1. Compared to the P25 TiO_2 support ($S_{BET} = 62\ m^2 g^{-1}$), the specific surface area of the Pt/TiO_2 catalyst ($S_{BET} = 59\ m^2 g^{-1}$) decreased after Pt loading. UV-Vis spectra of P25 TiO_2 and 0.1 wt% Pt/P25 are shown in Figure S3a and the bandgap energy of the catalysts was found to be 3.2 eV for P25 TiO_2 which reduced to 3.0 eV for Pt/TiO_2 (as shown in Table S1 and Figure S3.b) in agreement with previous reports.[19]

The P25 TiO_2 support showed no reducibility below 600 °C from the H_2-TPR analysis, as shown in Figure S4, whilst after Pt loading a reduction peak was observed for Pt/TiO_2 at ~120 °C attributed to the reduction of PtO_x crystallites to metallic Pt.[20] Additional reduction peaks were detected at 300–500 °C, representing reduction of Pt species interacting more strongly with the P25 support or Pt-TiO_x interface sites.[18b]

H_2 production of different catalytic photoreforming systems

Comparative experiments were performed to assess the rate of H_2 production from a range of bio derived substrates over the 0.1 wt% Pt/TiO_2 catalyst including cellulose, lignin, guaiacol and phenol. Control experiments under dark condition without UVA irradiation for cellulose, phenol, benzoquinone, hydroquinone, and catechol as well as photolysis experiments without the presence of the catalyst for phenol and benzoquinone were undertaken and none of these tests resulted in any H_2 production. Additionally, photocatalytic water splitting over the catalyst was performed resulting in very low H_2 production, i.e., 0.2 ± 0.05 μmol after the 5 h reaction, as shown in Figure 1a. The photoreforming of cellulose resulted in 31 ± 0.8 μmol of H_2 after 5 h. Conversely, using lignin, the H_2 generation was only 2.4 ± 0.46 μmol over 5 h.

Phenol and guaiacol are simple aromatic compounds with hydroxylated and methoxylated functionalities which are common to the hydroxyphenylpropanoid monolignol compounds giving rise to the syringyl (S), guaiacyl (G) and p-hydroxyphenyl (H) units in the polymerised lignin structure. Hydroxylated/methoxylated aromatic functionalities are also present in newly identified monolignols,[21] and, therefore, guaiacol and phenol were studied as model compounds to probe whether enhancing the decomposition of lignin towards monomeric compounds would improve H_2 production by photoreforming. Interestingly, H_2 production from the small hydroxylated/methoxylated aromatic molecules phenol and guaiacol was also small. Using guaiacol and phenol just 2.4 ± 0.36 μmol and 3.3 ± 0.62 μmol of H_2 was formed after 5 h of reaction, respectively. This result contrasts with cellulose photoreforming, in which H_2 production from the monomer glucose (and other sugars) is significantly higher than from the insoluble cellulose.[9b] In addition, the H_2 production from the aromatic photoreforming systems here was comparable to that in the literature for aromatic substrates of phenol,[22] naphthalene,[23]

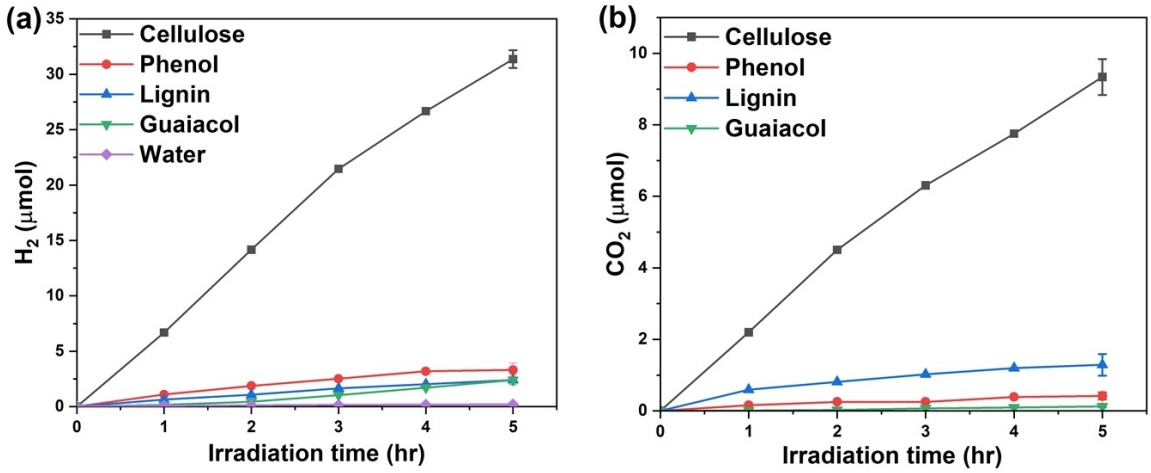

Figure 1. (a) H_2 production from the systems of photocatalytic water splitting and catalytic photoreforming of different bio-substrates over the 0.1 wt% Pt/TiO_2 catalyst; (b) CO_2 production from the catalytic photoreforming systems using different bio-substrates over the 0.1 wt% Pt/TiO_2 catalyst. Conditions: T = 40 °C; concentration of the catalyst = 1 mg ml^{-1}; concentrations of the bio-substrates: lignin = 0.1 mg ml^{-1}, guaiacol = 0.25 mg ml^{-1}, phenol = 0.25 mg ml^{-1} and cellulose = 1 mg ml^{-1}. Incident photon rate: 62.9 μmol h^{-1} photons, 1 mol (6.0223×10^{23}) is 1 Einstein of photons was titrated by a potassium ferrioxalate actinometre.[24]

and benzene,[22b] suggesting low activity of aromatic substrates under anaerobic photoreforming conditions.

CO_2 was found to be the major carbon-containg gaseous product (Figure 1b) together with trace levels of CH_4 produced by the systems based on phenol and guaiacol at 0.05 and 0.1 μmol, respectively, shown in Figure S5 and S6. Note that CH_4 was not detected in the photoreforming systems of lignin or cellulose. In line with the relative H_2 production values, the cellulose photoreforming system produced the highest amount of CO_2 at 9.3 ± 0.5 μmol, whilst that for lignin, phenol and guaiacol was 1.3 ± 0.3 μmol, 0.4 ± 0.1 μmol and 0.1 ± 0.03 μmol, respectively.

Phenol photoreforming under the same reaction conditions over bare P25 TiO_2 gave H_2 production of ~1.6 μmol, being only approximately two times lower than that over the 0.1 wt% Pt/TiO_2 catalyst, as shown in Figure S6. The results suggest that the promoting effect from loading Pt on the P25 TiO_2 on aromatic photoreforming is less significant compared to the system using cellulose as the substrate.[25] For example, a previous study showed that photoreforming of cellulose over m-TiO_2 produced ~1.2 μmol H_2 after 5 h reaction, whilst the system over the 0.08 wt% Pt/TiO_2 catalyst increased the H_2 production considerably to ~44.5 μmol.[25a] However, CO_2 production from phenol photoreforming over bare P25 TiO_2 (~1.1 μmol) was higher than that over 0.1 wt% Pt/TiO_2 (~0.5 μmol), as shown in Figure S6, indicating a lower extent of substrate/intermediate oxidation due to Pt acting as a charge recombination center in a low H^+ (electron scavenger) system as opposed to promoting charge separation.[23,26]

Figure 2 shows the colour change of different phenol reforming systems (after the 5-h reaction) from bare P25 TiO_2 under UV irradiation, from 0.1 wt% Pt/TiO_2 under dark conditions and from 0.1 wt% Pt/TiO_2 under UV irradiation. No colour changes were observed in the first two systems (Figures 2a and 2b). Conversely, for the system over 0.1 wt% Pt/TiO_2, an immediate darkening of the solution/catalyst mixture was observed upon exposure to UV irradiation (Figure 2c). Similar phenomena have been reported previously in naphthalene photoreforming[23] and benzene photoreforming[22b] over Pt/TiO_2 catalysts.

The colour change has been attributed to the formation of light absorbing intermediates in the liquid phase and the formation of phenoxy and polyphenyl species which strongly adsorbed on the surface of TiO_2.[22b] However, to date, limited studies on the interaction between the phenol partial oxidation intermediates and TiO_2, as well as their activity in photoreforming systems under anaerobic conditions,[27] have been reported.

Investigation of the intermediate-catalyst interactions

To understand the role of the intermediates in phenol photoreforming, hydroquinone, catechol and *p*-benzoquinone, which were identified by HPLC during the reaction, were compared for H_2 production over 0.1 wt% Pt/TiO_2. In each case, the production of H_2 was lower than found for phenol, for example, during hydroquinone photoreforming ~0.5 μmol H_2 was formed after 5 h, compared with ~3.3 μmol H_2 from phenol. Furthermore, the catechol and benzoquinone systems produced no H_2.

The absence of CO_2 and H_2 production using catechol is consistent with surface poisoning as a result of strong catechol adsorption on the TiO_2 support, as reported previously.[28] In order to examine this hypothesis and understand the differences between the substrates, the substrates were pre-adsorbed under dark conditions and then used in the photoreforming of cellulose. Figure 3 shows that the activity regarding H_2 production over the phenol pre-adsorbed catalyst was almost comparable to that of the fresh catalyst (~30.6 μmol) indicating no poisoning from the dark adsorption of phenol. However, the pre-adsorption of hydroquinone and benzoquinone reduced the H_2 production from cellulose to ~24.1 μmol after adsorption of hydroquinone and ~14.5 μmol after benzoquinone adsorption. The catalyst following catechol preadsorption produced no H_2 after 5 h, confirming that the strong catechol adsorption on the catalyst hinders photoreforming reactions significantly. This has been proposed to be due

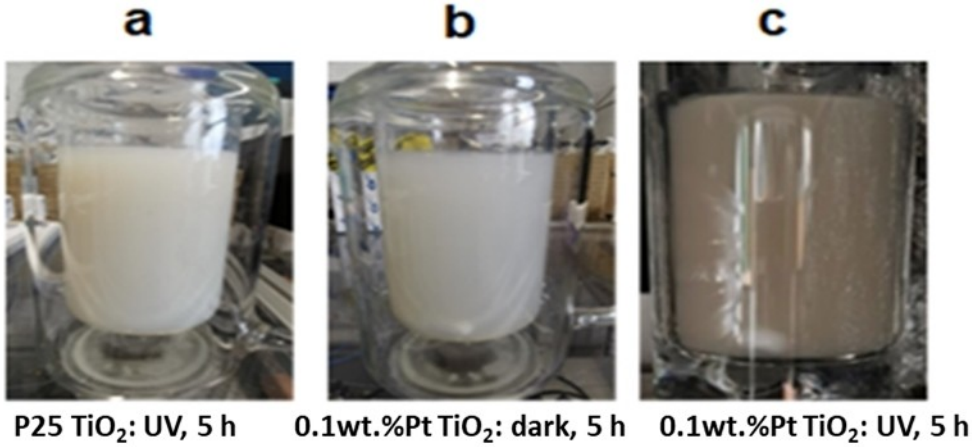

Figure 2. Colour of different phenol reforming systems over (a) P25 TiO_2 (1 mg ml^{-1}) under UV irradiation, (b) 0.1 wt% Pt/TiO_2 (1 mg ml^{-1}) under dark condition and (c) 0.1 wt% Pt/TiO_2 (1 mg ml^{-1}) under UV irradiation. Conditions: phenol concentration in the aqueous system = 0.25 mg ml^{-1}, reaction time = 5 h.

Research Article
doi.org/10.1002/cplu.202300411
Chemistry Europe
European Chemical Societies Publishing

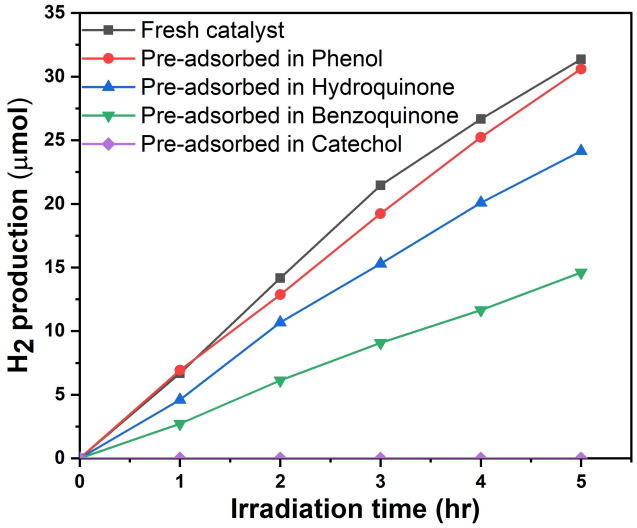

Figure 3. Comparison of H_2 evolution from catalytic photoreforming of cellulose over the fresh 0.1 wt% Pt/TiO_2 catalyst and the same catalyst when the substrate was pre-adsorbed (using phenol, hydroquinone, benzoquinone and catechol). Conditions: T = 40 °C; concentration of the catalyst = 1 mg ml^{-1}; concentrations of the cellulose: 1 mg ml^{-1}

electron transfer reactions between TiO_2 and the adsorbed catechol species under irradiation.[29] Interestingly, after dark adsorption of catechol on 0.1 wt% Pt/TiO_2, the same colour change to that of the phenol photoreforming system over 0.1% Pt/TiO_2 (Figure 2c) was observed, as shown in Figure S7, suggesting the strong adsorption of catechol. UV irradiation was not required to induce a colour change in the catechol-catalyst solution, whereas for hydroquinone-catalyst solution, a change in solution colour to brown was only observed upon irradiation in the presence of 0.1wt%Pt/TiO_2. For benzoquinone-catalyst solution, the solution colour changed to brown over P25 TiO_2 and to a greater degree over 0.1 wt%Pt/TiO_2 under UV irradiation (Figure S8). While a colour change in the catalyst/solution was not observed following the dark adsorption of hydroquinone and benzoquinone on 0.1 wt% Pt/TiO_2 their adsorption similarly had a negative effect on cellulose photoreforming which suggests stronger adsorption of these intermediates than phenol.

To probe the relative interaction strength of the intermediates with P25 TiO_2 and 0.1 wt% Pt/TiO_2, NMR relaxometry was used. Phenol/water adsorption on the support and catalyst was performed as well for comparison. Table 2 shows the values for the NMR relaxation time ratio T_1/T_2 for the interactions between different probe molecules and P25 TiO_2/0.1 wt% Pt/TiO_2. The dimensionless ratio T_1/T_2 of the longitudinal-to-transverse nuclear spin relaxation times is known to be proportional to the strength of the interaction between the probe molecule and the surface of the solid, as shown by several studies.[30]

The trend in the T_1/T_2 values over the 0.1 wt% Pt/TiO_2 showed weakest adsorption for phenol and water with values of 8.7 and 7.7, respectively (Table 2 and Figure S9). All other intermediates were more strongly adsorbed on 0.1 wt% Pt/TiO_2 than water (and phenol) with catechol the most strongly adsorbed with a significantly higher T_1/T_2 value of 16.2, in line

Table 2. T_1/T_2 interaction strengths value (average of two experiments) for water, phenol, catechol, hydroquinone and *p*-benzoquinone over P25 TiO_2 and 0.1 wt% Pt/TiO_2.

Substrate	*Support/catalyst*	
	P25 TiO_2	0.1 wt% Pt/TiO_2
Water	10±0.2	8.7 ± 0.7
Phenol	10.1 ± 0.4	7.7 ± 0.6
Hydroquinone (HQ)	9.5 ± 0.2	9.3 ± 0.5
p-Benzoquinone (BQ)	11.5 ± 0.4	10.0 ± 0.0
Catechol	14.0 ± 0.4	16.2 ± 0.35

with the strong poisoning effect observed (Figure 3). Weaker adsorption was observed for hydroquinone and benzoquinone at 9.3 and 10.0, being more comparable to the adsorption of water. In the case of the P25 TiO_2 system, it was found that the T_1/T_2 value of phenol (10.1) had a similar adsorption strength to water (10.0) with benzoquinone and catechol adsorbing more strongly with T_1/T_2 values of 11.5 and 14.0, respectively, as shown in Table 2 and Figure S9. The trend in the strength of substrate/intermediate adsorption on 0.1 wt% Pt/TiO_2 determined from NMR relaxometry correlated with their effect on cellulose photoreforming observed following dark adsorption. As the T_1/T_2 values increased, the H_2 production from cellulose was found to decrease.

ATR-IR spectra was also used to study the adsorption catechol and phenol over the P25 TiO_2 catalysts. The P25 TiO_2 exposed to a solution of 0.1 M catechol in water showed formation of a bidentate catecholate species with bands at 1480 cm^{-1} (ν(C–C) of aromatic ring) and 1249 cm^{-1} (ν(C–O)).[31] The comparable system with P25 TiO_2 exposed to phenol, however, only showed bands due to a physiorbed species with no significant difference in the spectra over the blank crystal and the P25 TiO_2 catalyst (Figure 4). The nature of the substrate adsorption correlates with the adsorption strengths from NMR relaxometry, with the differing adsorption strengths for phenol and catechol (relative to water) resulting in predominantly

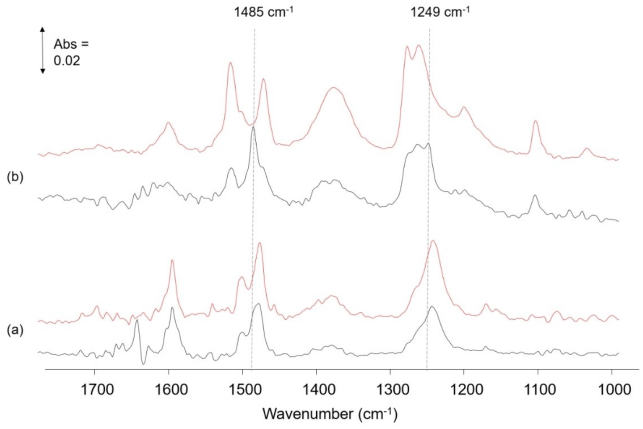

Figure 4. ATR-IR spectra of (a) 0.1 M phenol in water and (b) 0.1 M catechol in water over P25 TiO_2 (black spectra) and ZnSe crystal (red spectra) at room temperature. Bands due to water have been subtracted from the spectra.

physiorbed and chemisorbed species, respectively. Previous FTIR studies showed a water induced change in phenol adsorption from a dissociatively adsorbed phenolate (on a dehydroxylated P25 surface) to a physiorbed molecular species[32] and formation of chemisorbed catecholate species from adsorption of catechol on TiO_2 in aqueous systems.[33] In addition, Doménech et al. found the adsorption constant for catechol to be approximately two times higher than phenol on P25 catalysts using a Langmuir-Hinshelwood kinetic model.[34]

Chemisorbed catecholate on TiO_2 (bidentate adsorption) has been reported to react with the photogenerated holes (forward electron transfer) to form the radical cation $Cat^{+\bullet}$ which has been shown to undergo charge recombination ($Cat^{+\bullet} + e^- = Cat$, back electron transfer) scavenging electrons.[35] Fast recombination of electrons and holes quenches the charge separation and subsequent oxidation reactions (to form CO_2) and electron migration to Pt centres for proton reduction reactions (forming H_2). Kaniyankandy et al.[36] performed femtosecond transient absorption spectroscopy of catechol, resourcinol and hydroquinone in TiO_2 systems to probe localised/delocalised electron transfer dynamics. It was found that the rate of forward electron transfer was comparable for catechol, resourcinol and hydroquinone, whilst the rate of the back electron transfer (recombination reactions) was fastest for catechol. This was due to the positioning of the bridging ligands on the aromatic ring and the distance between the Ti adsorption centres in the respective bidentate chemisorbed species. As the distance between the Ti centres increased (catechol to resourcinol to hydroquinone) the rate of charge recombination decreased due to increased delocalisation of the injected electron over several Ti centres. While no H_2 was formed from the catechol photoreforming system, a small amount of H_2 was formed from hydroquinone which has a lower rate of charge recombination. Phenol does not undergo back electron transfer recombination reactions and exhibited higher H_2 production than from the systems using catechol and hydroquinone.

The lack of H_2 during catechol photoreforming can be explained by strong surface adsorption of the substrate however for benzoquinone the T_1/T_2 value was significantly lower than found for catechol. This suggests benzoquinone adsorption strength was not the factor hindering H_2 production. In this case, during the photoreforming reaction over 0.1 wt% Pt/TiO_2, benzoquinone was reduced to hydroquinone resulting in 0.11 mg ml^{-1} being produced after 5 h with 0.12 mg ml^{-1} of benzoquinone being converted. Reduction of benzoquinone to hydroquinone was also found using Pd–Au/TiO_2 catalysts under anaerobic conditions, as well as in the catalyst-free aqueous system under UV irradiation.[37] Herein, benzoquinone conversion under photolysis conditions (i.e., under UV irradiation without a catalyst) was also measured resulting in the formation of hydroquinone (~0.03 mg ml^{-1}) and CO_2 (6.5 μmol), as well as short chain carboxylic acids (such as oxalic acid) and other unidentified compounds (Figure S10, quantitative analysis of the reaction mass balance was not possible due to the overlapping peaks). Hence, in the current system with 0.1 wt% Pt/TiO_2 (and P25 TiO_2), the pathway for the transformation of benzoquinone to hydroquinone dominates under the photoreforming condition, whilst direct photolysis and surface oxidation reactions (of benzoquinone or short chain acid photolysis products forming CO_2) were less prevalent over the catalyst. It is worth noting that the TiO_2 catalysed benzoquinone reduction to hydroquinone could reduce the overall efficiency of the phenol photoreforming reactions since benzoquinone reduction consumes the photogenerated electrons.[37–38] In this case, the benzoquinone reduction to hydroquinone, which requires $2e^-$ and $2H^+$, competes directly with the H_2 production reaction, and hence the oxidation of aromatic substrates anaerobically could be hindered upon formation of benzoquinone in the oxidation pathway (Scheme 1).

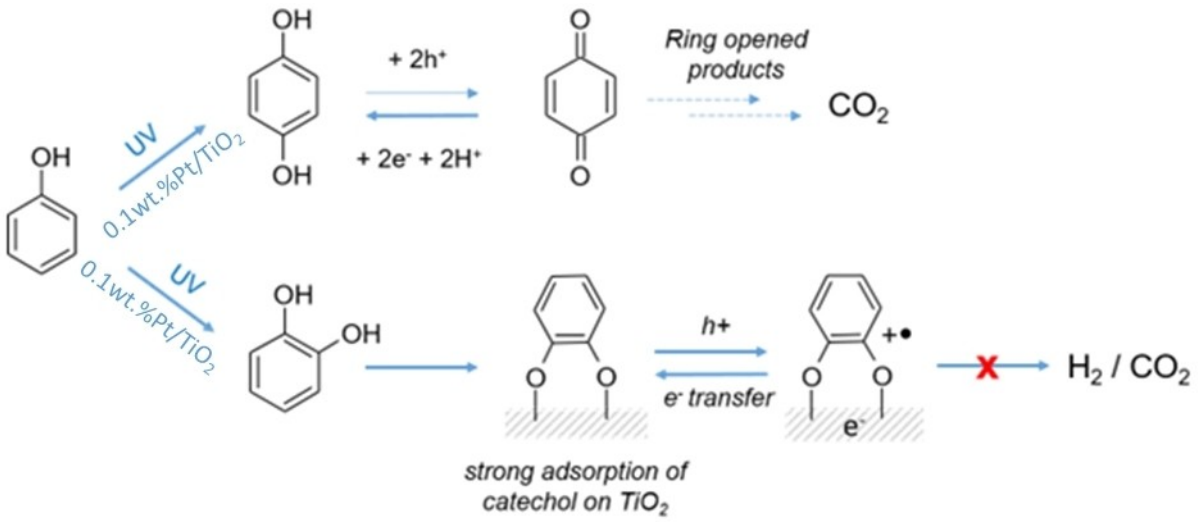

Scheme 1. The proposed reaction pathway of phenol photoreforming over the 0.1 wt% Pt/TiO_2 catalyst.

A new proposal to improve lignin photoreforming towards H_2 production

The findings from this study suggest that the presence of the oxidised intermediates (such as catechol and benzoquinone from phenol oxidation) could reduce the photocatalytic efficiency of the lignin photoreforming system considerably due to the strong adsorption (on TiO_2, most likely at Pt-TiO_2 interface sites[24]) and competing electron/proton transfer reactions. Hence, a possible strategy to mitigate such adverse effects could be a cyclic operation between anaerobic (H_2 production stage) and aerobic (regeneration/ring opening) conditions over the 0.1 wt%Pt/TiO_2 catalyst. O_2 was known to be beneficial to photocatalytic aromatic ring opening,[39] and thus aerobic conditions (i.e., photooxidation) could facilitate ring opening of the aromatic intermediates to form compounds more amenable to photoreforming and remove strongly adsorbed intermediates (regenerating the catalyst and overcoming the barrier in the oxidation pathway (benzoquinone oxidation as opposed to reduction) to form acids and ultimately CO_2).

Using this strategy, photoreforming of organosolv lignin was performed for 2 h with intervals of treatment of the catalyst with 30 min O_2/UV between the anaerobic photoreforming reactions. As shown in Figure 5, the cyclic operation was shown to improve the H_2 production significantly from the lignin photoreforming system. The initial H_2 production from the first 2-h photoreforming cycle was only ~1.0 μmol (corresponding to a H_2 production rate of 5 $\mu mol\,h^{-1}\,g_{cat}^{-1}$). After the first aerobic O_2/UV treatment, H_2 production of the following anaerobic photoreforming increased to ~2.4 μmol (i.e., 11 $\mu mol\,h^{-1}\,g_{cat}^{-1}$) with a further increase to ~3.2 μmol (i.e., 16 $\mu mol\,h^{-1}\,g_{cat}^{-1}$) upon the second O_2/UV treatment. In addition, the colour of the system was observed to be reduced in intensity after the 30 min aerobic treatments, as shown in Figure S11, suggesting the oxidative removal of surface-adsorbed intermediates by the O_2/UV treatment.

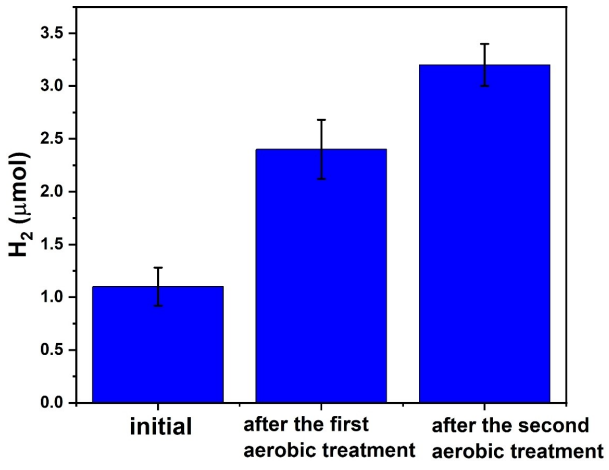

Figure 5. H_2 production from the alternative anaerobic-aerobic (photoreforming-regenration) system over the 0.1 wt% Pt/TiO_2 catalyst. Conditions: T = 40 °C, lignin concentration = 0.1 mg ml^{-1}; catalyst concentration = 1 mg ml^{-1}; O_2 flow = 40 ml min^{-1}).

Conclusions

Photoreforming of lignin has the potential to serve as a promising platform for the simultaneous production of green H_2 and value-added chemicals, however, this process remains challenging. Here, lignin and lignin monomer model compounds (phenol and guaiacol) were photoreformed under ambient conditions in a pH-neutral aqueous solution (over P25 TiO_2 and 0.1 wt% Pt/TiO_2) to gain the mechanistic understanding of lignin photoreforming.

The results show a comparable evolution of H_2 from photoreforming of lignin and its model compounds, being significantly lower than from the control using cellulose, due to the intermediates formed (via the aromatic oxidation pathway), which reduced the photocatalytic efficiency of the system. During phenol photoreforming the interaction of intermediates (i.e., benzoquinone and catechol) with the catalysts, lead to catalyst poisoning from strong adsorption and electron transfer reactions reducing H_2 production. To address this challenge, a cyclic anaerobic-aerobic operation was proposed, which could enable alternative photoreforming-regeneration cycles to enhance H_2 production from lignin photoreforming, especially, in the aerobic cycle which could oxidise the adsorbed intermediates on the catalyst surface to recover the catalyst activity. The proof-of-concept of the cyclic anaerobic-aerobic process for improving H_2 production from aromatic substrates/lignin photoreforming shows a threefold improvement, and further development of such systems under flow conditions using Taylor flow photo reactors could be a promising approach to further increase H_2 yields.

Experimental

Chemicals and Materials

The TiO_2 (P25) support was purchased from Evonik. The Pt precursor, chloroplatinic acid hexahydrate ($H_2PtCl_6 \cdot 6H_2O$, 37.5% Pt assay), was purchased from Honeywell Fluka. Guaiacol (≥ 99%) and phenol (≥ 99%) were used as the lignin model-compounds and obtained from Acros Organic and Sigma-Aldrich, respectively and were used as received. The organosolv lignin obtained from *platycodon grandiflorum* (a herbaceous flowering perennial plant) and *corn stigmata maydis*, was purchased from Chemical Point (CAS no. 8068-03-9) and used as received.[40] The microcrystalline cellulose was purchased Sigma-Aldrich. Benzoquinone (≥ 99.5%), hydroquinone (≥ 99.5%), and catechol (≥ 99%) were purchased from Sigma-Aldrich and used as received. Deionised water was obtained from the Direct-Q 3UV ultrapure water system (Millipore).

Catalyst preparation

The Pt/TiO_2 photocatalyst was prepared by a wet impregnation method with a Pt loading of 0.1 wt% which was shown to be the optimum loading in the photoreforming of cellulose under comparable reaction conditions.[25a] In detail, 1 g of powder P25 was suspended in 10 ml of distilled water and stirred for 15 min at room temperature before the required amount 0.2 ml of the metal precursor solution (H_2PtCl_6) (0.01 g L^{-1}) was added dropwise to the TiO_2 slurry to achieve the metal loading (0.1 wt%), and the mixture

was stirred at 60 °C for 3 h. The resulting slurry was then dried at 150 °C for 2 h in an oven and calcined at 500 °C for 2 h under static air. The resulting dried powder was reduced in a tubular furnace under a pure hydrogen flow at 100 ml min^{-1} for 1 h at 200 °C and ground by agate mortar before catalysis.

Characterisation of materials

The physicochemical properties of TiO_2 P25 and the 0.1 wt% Pt/TiO_2 photocatalyst were characterised by Powder X-ray diffraction (PXRD), N_2 adsorption-desorption, inductively coupled plasma optical emission spectroscopy (ICP-OES), UV-vis, and hydrogen temperature-programmed reduction (H_2-TPR).

PXRD was conducted using a PANalytical 'X'Pert Pro (XRD5) instrument. Cu K_α radiation (λ = 1.5406 Å) was used operating at 40 kV and 40 mA, and the diffraction patterns were obtained between 2θ from 10° to 90° with a step size of 0.0335°. The Scherrer equation was used to estimate the crystallite sizes (D, nm) of the anatase (101) and rutile (110) reflections using a dimensionless shape factor (k_d = 0.943). The anatase/rutile ratio was calculated using Eq. (1) and considering the anatase (101) and rutile (110) reflection intensities, at 2θ values of 25.3° and 27.4°, respectively.

$$A(\%) = \frac{(100 \times I_A)}{I_A + 1.265 \times I_R} \quad (1)$$

where A (%) is the percentage of anatase, I_A and I_R represent the intensity of the anatase (101) and rutile (110) reflections, respectively.

N_2 physisorption performed using Quantachrome Autsorb IQ instrument, and the specific surface area of the materials was determined using the Brunauer-Emmett-Teller (BET) method. The actual Pt loading on the catalyst was measured by ICP-OES (PlasmaQuant PQ 9000 Elite). Before the ICP-OES analysis, the ETHOS EASY microwave digester was used to digest the catalysts using 12 ml aqua regia (9 ml HCl: 3 ml HNO_3) at 220 °C for 20 min. The bandgap energy of the photocatalyst was determined by UV-vis using a Praying Mantis Diffuse Reflectance accessory housed in a Shimadzu UV-2600 spectrophotometer. MgO powder was used as the background, and the spectra were recorded between 200–800 nm. The photocatalysts absorbance and band gap energy were determined using the Tauc plot method applied by the Kubelka-Munk model. H_2-TPR analysis of the catalyst (~100 mg) was measured under a 5% H_2/Ar flow at 40 ml min^{-1} between 30 °C and 800 °C with a heating rate of 10 °C min^{-1}. H_2 consumption during the analysis was measured by a thermal conductivity detector (TCD) in the QuantaChrom ChemBET Pulsar TPR/TPD Analyser. Scanning transmission electron microscopy (STEM) was performed using a probe aberration corrected FEI Titan G2 80–200 ChemiSTEM operated at 200 kV. High-resolution high angle annular dark field (HAADF) images were collected using 110 pA beam current, 21 mrad convergence angle and a 48 mrad HAADF collection inner angle. Powdered catalysts samples were prepared for STEM via dropcasting on a holey carbon support grid from methanol solution.

Photocatalytic reactions

Photocatalytic reactions were carried out in a borosilicate glass photoreactor comprised of a flat bottom, to facilitate the stirring during the reaction and a jacket for flowing water to regulate the reactor temperature. There were four ports on the top of the reactor for gas purging, removal of liquid samples for analysis by HPLC, connection to an online gas chromatography (GC) and a vent line.

Typically, 100 mg of the catalyst (Pt/TiO_2) and 0.25 mg ml^{-1} of substrates (guaiacol, phenol, benzoquinone, hydroquinone, and catechol), 1 mg ml^{-1} of cellulose or 0.1 mg ml^{-1} of lignin were suspended in 100 ml of distilled water. This mixture was stirred while purging with Ar for 30 min at room temperature to remove dissolved oxygen from the system. Before illumination, a water circulation bath flowed water to the jacket to control the reaction temperature at 40 °C. The reactor was sealed, and the light was switched on, irradiating the reactor with a UV-A lamp (365 nm, 2×8 W, supplied by Thistle Scientific). The gases produced from the reaction were carried in an Ar flow periodically to the GC to analyse the gas products (H_2, CO, CO_2 and CH_4). The GC (Perkin Elmer Clarus 580 GC) was fitted with a TCD and flame ionisation detector (FID with methaniser) with two columns, i.e., a 2 m inline HayeSep DB 100/120 mesh column followed by a 2 m ShinCarbon ST 100/120 mesh column.

Photoreforming of cellulose was also performed after the (dark) pre-adsorption at room temperature of phenol, hydroquinone, benzoquinone and catechol (0.25 mg ml^{-1} in water) over the 0.1 wt% Pt/TiO_2 (1 mg ml^{-1}). The catalysts were recovered after 5 h in the respective substrate solution, centrifuged and dried before use.

Photoreforming of lignin (0.1 mg ml^{-1}) and phenol (0.1 and 0.05 mg ml^{-1}) was also conducted under alternating anaerobic and aerobic atmospheres, as illustrate by Figure S12. The photoreforming for lignin and phenol was carried out for 2 h (anaerobic environment) before and after treatments under O_2/UV (40 ml min^{-1}, UVA lamp as for anaerobic reaction) for 30 min and the gas phase products were analysed by GC during each stage.

Liquid samples from the photocatalytic systems were analysed by high-performance liquid chromatography (HPLC, an Agilent 1220 Infinity LC system with a diode array detector emitting in the UV range with a Syncronis TM C18 column) to determine relevant substrate conversions and identify relevant products in the liquid phase after the photoreforming reactions. The HPLC conditions were UV wavelength = 254–320 nm, oven temperature = 60 °C, sample injection volume = 5 μL and flow rate = 0.6 ml min^{-1}. The mobile phase for analysis was water-acetonitrile solvent 95.0 : 5.0, v/v. HPLC was also performed using a Bio-Rad Aminex HPX-87H ion exclusion column (300 mm×7.8 mm). The temperature of column oven was 50 °C, and the mobile phase was 0.005 mol L^{-1} H_2SO_4 in HPLC grade water at a flow rate of 0.6 ml min^{-1}.

NMR relaxometry

For the NMR relaxation measurements, a Spinsolve™ low-field instrument was used in this study to identify the strength of the interaction between the substrates (of phenol, hydroquinone, catechol and benzoquinone) and the catalyst surface. The pure P25 TiO_2 support or 0.1 wt% Pt/TiO_2 samples (~100 mg powder) were soaked overnight to fully saturate their pores with the selected liquids (water or 0.25 mg ml^{-1} of the substrates above). Before the measurements, the powders were removed from the liquid, and dried carefully using filter papers to remove any liquid on the external surfaces between the solid grains, so that only the liquid residing inside the pores of the solids was monitored. A typical T_1/T_2 pulse sequence was used, as shown in Figure S13.

The pulse sequence was repeated 16 times for each measurement, for 16 different delay times, from 1 ms up to 3000 ms, separated by log-spaced intervals. The echo time was 100 μs and the number of echoes was 4096. The raw relaxation data obtained by these

measurements have been processed using a numerical inversion computer algorithm,[41] in order to obtain 2D maps with the T_1 and T_2 relaxation time distributions as their axes. Using weighted average methods, the T_1 and T_2 time constants of the sample can be calculated from the 2D maps.

In these NMR experiments, the relaxation time results are the average between the relaxation times of the protons in the water molecules, and the protons in the solutes. Since the concentration of the solvents is very low, it is hard to distinguish between the two and study them individually. However, the average relaxation times shift considerably when the solutes are introduced to the system, and thus we can interpret this shift as the result of the interactions between the solutes and the surface sites of the catalyst.

ATR-IR spectroscopy

Attenuated total reflectance (ATR) spectroscopy was utilised to probe the mode of adsorption of phenol and catechol in aqueous solution, over P25 TiO_2. ATR-IR spectra were recorded using an in-house modified ATR flow cell in a PIKE ATRMaxII accessory housed in a Bruker Tensor II spectrometer. P25 TiO_2 layers were prepared by depositing a slurry of P25 TiO_2 in water onto a ZnSe crystal and evaporating to dryness at room temperature overnight. Spectra were recorded (8 scans, resolution of 4 cm^{-1}) under a flow of 0.1 M phenol or catechol in water over the catalyst at room temperature and the background spectrum was the catalyst layer before its exposure to any solution.

Acknowledgements

M.A. thanks the King Abdulaziz City for Science and Technology for the scholarship to support his PhD research at The University of Manchester. The authors thank the EPSRC-funded Supergen Bioenergy Hub (EP/S000771/1) for funding this research. UK Catalysis Hub is kindly thanked for resources and support provided via our membership of the UK Catalysis Hub Consortium and funded by EPSRC grants: EP/R026939/1, EP/R026815/1, EP/R026645/1 and EP/R027129/1. TEM access was supported by the Henry Royce Institute for Advanced Materials, funded through EPSRC grants EP/R00661X/1, EP/S019367/1, EP/P025021/1, EP/P025498/1 and EP/S021531/1. This project has received funding from the European Union's Horizon 2020 research and innovation program under grant agreement No 872102.

Conflict of Interests

The authors declare no conflict of interest.

Data Availability Statement

The data that support the findings of this study are available in the supplementary material of this article.

Keywords: adsorption · hydrogen (H_2) · lignin · phenol · photoreforming

[1] a) C. Acar, I. Dincer, *J. Cleaner Prod.* **2019**, *218*, 835–849; b) T. M. Letcher in *Future Energy*, (Eds.: T. M. Letcher), Elsevier, Amsterdam, **2020**, pp. 3–17.
[2] M. Voldsund, K. Jordal, R. Anantharaman, *Int. J. Hydrogen Energy* **2016**, *41*, 4969–4992.
[3] S. E. Hosseini, M. A. Wahid, *Renewable Sustainable Energy Rev.* **2016**, *57*, 850–866.
[4] a) M. F. Kuehnel, E. Reisner, *Angew. Chem. Int. Ed. Engl.* **2018**, *57*, 3290–3296; b) C. Shi, F. Kang, Y. Zhu, M. Teng, J. Shi, H. Qi, Z. Huang, C. Si, F. Jiang, J. Hu, *Chem. Eng. J.* **2022**, 138980.
[5] T. Uekert, C. M. Pichler, T. Schubert, E. Reisner, *Nat. Sustain* **2020**.
[6] S. H. Shinde, A. Hengne, C. V. Rode in *Recent Advances in Development of Platform Chemicals*, (Eds.: S. Saravanamurugan, A. Pandey, H. Li, A. Riisager), Elsevier, Amsterdam, **2020**, pp. 1–31.
[7] G. Gellerstedt, G. Henriksson in *Monomers, Polymers and Composites from Renewable Resources*, (Eds.: M. N. Belgacem, A. Gandini), Elsevier, Amsterdam, **2008**, 201–224.
[8] S. Haghdan, S. Renneckar, G. D. Smith in *Lignin in Polymer Composites*, (Eds.: O. Faruk, M. Sain), Elsevier, Amsterdam, **2016**, pp. 1–11.
[9] a) X. Fu, J. Long, X. Wang, D. Y. C. Leung, Z. Ding, L. Wu, Z. Zhang, Z. Li, X. Fu, *Int. J. Hydrogen Energy* **2008**, *33*, 6484–6491; b) A. Caravaca, W. Jones, C. Hardacre, M. Bowker, *Proc Math Phys Eng Sci* **2016**, *472*, 20160054.
[10] a) V. M. Daskalaki, D. I. Kondarides, *Catal. Today* **2009**, *144*, 75–80; b) E. A. Kozlova, A. Y. Kurenkova, E. Y. Gerasimov, N. V. Gromov, T. B. Medvedeva, A. A. Saraev, V. V. Kaichev, *Mater. Lett.* **2021**, *283*, 128901.
[11] a) G. Zhang, C. Ni, X. Huang, A. Welgamage, L. A. Lawton, P. K. Robertson, J. T. Irvine, *Chem. Commun. (Camb.)* **2016**, *52*, 1673–1676; b) C. Chang, N. Skillen, S. Nagarajan, K. Ralphs, J. T. Irvine, L. Lawton, P. K. Robertson, *Sustain. Energy Fuels* **2019**, *3*, 1971–1975.
[12] T. Sakata, T. Kawai, *J. Synth. Org. Chem. Jpn.* **1981**, *39*, 589–602.
[13] a) D. W. Wakerley, M. F. Kuehnel, K. L. Orchard, K. H. Ly, T. E. Rosser, E. Reisner, *Nat. Energy* **2017**, *2*; b) H. Kasap, D. S. Achilleos, A. Huang, E. Reisner, *J. Am. Chem. Soc.* **2018**, *140*, 11604–11607; c) H. Zhao, C.-F. Li, L.-Y. Liu, B. Palma, Z.-Y. Hu, S. Renneckar, S. Larter, Y. Li, M. G. Kibria, J. Hu, B.-L. Su, *J. Colloid Interface Sci.* **2020**; d) C. Rao, M. Xie, S. Liu, R. Chen, H. Su, L. Zhou, Y. Pang, H. Lou, X. Qiu, *ACS Appl. Mater. Interfaces* **2021**, *13*, 44243–44253; e) H. Nagakawa, M. Nagata, *Adv. Mater. Interfaces* **2022**, *9*, 2101581; f) E. Wang, A. Mahmood, S.-G. Chen, W. Sun, T. Muhmood, X. Yang, Z. Chen, *ACS Catal.* **2022**, *12*, 11206–11215.
[14] C. Li, H. Wang, S. B. Naghadeh, J. Z. Zhang, P. Fang, *Appl. Catal. B* **2018**, *227*, 229–239.
[15] S. Guadix-Montero, M. Sankar, *Top. Catal.* **2018**, *61*, 183–198.
[16] G. R. Hafenstine, R. E. Patalano, A. W. Harris, G. Jiang, K. Ma, A. P. Goodwin, J. N. Cha, *ACS Appl. Polym. Mater.* **2019**, *1*, 1451–1457.
[17] a) K. Doudrick, O. Monzón, A. Mangonon, K. Hristovski, P. Westerhoff, *J. Environ. Eng.* **2012**, *138*, 852–861; b) B. Ohtani, O. Prieto-Mahaney, D. Li, R. Abe, *J. Photochem. Photobiol. A* **2010**, *216*, 179–182.
[18] a) L. Qin, G. Wang, Y. Tan, *Sci. Rep.* **2018**, *8*, 1–13; b) S. Kuhaudomlap, O. Mekasuwandumrong, P. Praserthdam, S.-I. Fujita, M. Arai, J. Panpranot, *Catalysts* **2018**, *8*.
[19] E. Kowalska, H. Remita, C. Colbeau-Justin, J. Hupka, J. Belloni, *J. Phys. Chem. C* **2008**, *112*, 1124–1131.
[20] C. Zhang, H. He, K.-i. Tanaka, *Appl. Catal. B* **2006**, *65*, 37–43.
[21] R. C. Sun, *ChemSusChem* **2020**, *13*, 4385–4393.
[22] a) D. Li, J. C.-C. Yu, V.-H. Nguyen, J. C. S. Wu, X. Wang, *Appl. Catal. B* **2018**, *239*, 268–279; b) H. Yuzawa, M. Aoki, K. Otake, T. Hattori, H. Itoh, H. Yoshida, *J. Phys. Chem. C* **2012**, *116*, 25376–25387.
[23] O. Al-Madanat, Y. AlSalka, R. Dillert, D. W. Bahnemann, *Catalysts* **2021**, *11*, 107.
[24] L. Lan, H. Daly, R. Sung, F. Tuna, N. Skillen, P. K. Robertson, C. Hardacre, X. Fan, *ACS Catal.* **2023**, *13*, 8574–8587.
[25] a) L. Lan, Y. Shao, Y. Jiao, R. Zhang, C. Hardacre, X. Fan, *Chin. J. Chem. Eng.* **2020**, *28*, 2084–2091; b) A. Speltini, M. Sturini, D. Dondi, E. Annovazzi, F. Maraschi, V. Caratto, A. Profumo, A. Buttafava, *Photochem. Photobiol. Sci.* **2014**, *13*, 1410–1419.
[26] a) B. Sun, A. V. Vorontsov, P. G. Smirniotis, *Langmuir* **2003**, *19*, 3151–3156; b) D. Benz, K. M. Felter, J. Köser, J. Thöming, G. Mul, F. C. Grozema, H. T. Hintzen, M. T. Kreutzer, J. R. Van Ommen, *J. Phys. Chem. C* **2020**, *124*, 8269–8278.
[27] J. Kim, W. Choi, *Energy Environ. Sci.* **2010**, *3*, 1042–1045.
[28] a) M. K. Abugazleh, B. Rougeau, H. Ali, *J. Environ. Chem. Eng.* **2020**, *8*, 104180; b) K. Lv, X. Guo, X. Wu, Q. Li, W. Ho, M. Li, H. Ye, D. Du, *Appl. Catal. B* **2016**, *199*, 405–411.

[29] T. Tachikawa, Y. Takai, S. Tojo, M. Fujitsuka, T. Majima, *Langmuir* **2006**, *22*, 893–896.
[30] a) C. D'Agostino, J. Mitchell, M. D. Mantle, L. F. Gladden, *Chem. Eur. J.* **2014**, *20*, 13009–13015; b) D. Weber, J. Mitchell, J. McGregor, L. F. Gladden, *J. Phys. Chem. C* **2009**, *113*, 6610–6615.
[31] H. Gulley-Stahl, P. A. Hogan, W. L. Schmidt, S. J. Wall, A. Buhrlage, H. A. Bullen, *Environ. Sci. Technol.* **2010**, *44*, 4116–4121.
[32] L. Mino, A. Zecchina, G. Martra, A. M. Rossi, G. Spoto, *Appl. Catal. B* **2016**, *196*, 135–141.
[33] P. Z. Araujo, P. J. Morando, M. A. Blesa, *Langmuir* **2005**, *21*, 3470–3474.
[34] A. M. Peiró, J. A. Ayllón, J. Peral, X. Doménech, *Appl. Catal. B* **2001**, *30*, 359–373.
[35] Y. Wang, K. Hang, N. A. Anderson, T. Lian, *J. Phys. Chem. B* **2003**, *107*, 9434–9440.
[36] S. Kaniyankandy, S. Rawalekar, A. Sen, B. Ganguly, H. N. Ghosh, *J. Phys. Chem. C* **2012**, *116*, 98–103.
[37] R. Su, R. Tiruvalam, Q. He, N. Dimitratos, L. Kesavan, C. Hammond, J. A. Lopez-Sanchez, R. Bechstein, C. J. Kiely, G. J. Hutchings, *ACS Nano* **2012**, *6*, 6284–6292.
[38] M. A. Henderson, M. Shen, *Top. Catal.* **2017**, *60*, 440–445.
[39] a) X. Pang, W. Chang, C. Chen, H. Ji, W. Ma, J. Zhao, *J. Am. Chem. Soc.* **2014**, *136*, 8714–8721; b) E. Szabó-Bárdos, O. Markovics, O. Horváth, N. Törő, G. Kiss, *Water Res.* **2011**, *45*, 1617–1628.
[40] a) C. Rodríguez Correa, M. Stollovsky, T. Hehr, Y. Rauscher, B. Rolli, A. Kruse, *ACS Sustainable Chem. Eng.* **2017**, *5*, 8222–8233; b) R. Süss, G. Aufischer, L. Zeilerbauer, B. Kamm, G. Meissner, H. Spod, C. Paulik, *Catal. Commun.* **2022**, *170*, 106503.
[41] a) J. Mitchell, T. Chandrasekera, L. Gladden, *Prog. Nucl. Magn. Reson. Spectrosc.* **2012**, *62*, 34–50; b) Y.-Q. Song, L. Venkataramanan, M. Hürlimann, M. Flaum, P. Frulla, C. Straley, *J. Magn. Reson.* **2002**, *154*, 261–268.

Manuscript received: July 31, 2023
Revised manuscript received: September 28, 2023
Accepted manuscript online: October 13, 2023
Version of record online: October 13, 2023

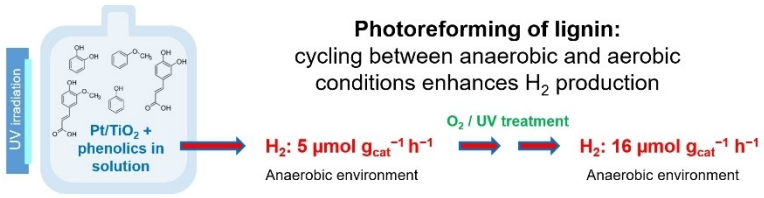

Lignin and aromatic model compounds (phenol and guaiacol) show low activity in the production of H_2 by photoreforming. Strong adsorption of intermediates (partial oxidation products) and electron transfer reactions inhibit the photocatalytic reactions under anaerobic conditions. Cycling between an anaerobic and a regenerative aerobic stage enhanced H_2 production from lignin.

M. Aljohani, Dr. H. Daly, Dr. L. Lan, A. Mavridis, Dr. M. Lindley, Prof. S. J. Haigh, Dr. C. D'Agostino, Dr. X. Fan*, Prof. C. Hardacre**

1 – 11

Enhancing Hydrogen Production from the Photoreforming of Lignin